

# Optical polarimetry and infrared photometry of two AM Her binaries: 1RXS J161008.0+035222 and 1RXS J231603.9–052713 <sup>\*</sup>

C. V. Rodrigues,<sup>1,†</sup> F. J. Jablonski,<sup>1</sup> F. D’Amico,<sup>1</sup> D. Cieslinski,<sup>1</sup> J. E. Steiner,<sup>2</sup>  
M. P. Diaz,<sup>2</sup> and G. R. Hickel<sup>3</sup>

<sup>1</sup> Instituto Nacional de Pesquisas Espaciais/MCT – Av. dos Astronautas, 1758 – 12227-010 - São José dos Campos - SP – Brazil

<sup>2</sup> Instituto de Astronomia, Geofísica e Ciências Atmosféricas/USP – Rua do Matão, 1226 – 05508-900 - São Paulo - SP – Brazil

<sup>3</sup> IP&D - Universidade do Vale do Paraíba – Av. Shishima Hifumi, 2911 – 12244-000 - São José dos Campos - SP – Brazil

30 April 2019

## ABSTRACT

We present the first optical circular and linear polarization measurements of two polar candidates from *ROSAT*: 1RXS J161008.0+035222 and 1RXS J231603.9–052713. We also present *H* band near-infrared photometry of the last object. The presence of strong circular polarization confirms them as AM Her systems. 1RXS J231603.9–052713 was observed in two different brightness states. The orbital phase dependence of the flux and polarization of 1RXS J161008.0+035222 is reasonably fitted with a simple model in which the binary is observed at a small inclination and the magnetic field axis is almost parallel to the white-dwarf rotation axis resulting in the accretion column axis being seen from top during the whole orbital revolution. An alternative geometry with intermediate inclination can fit the observed flux and circular polarization. However, in this case, the model produces a linear polarization peak which is not corroborated by the data. The estimated magnetic field is in the 10 to 20 MG range. The circular polarization of 1RXS J231603.9–052713 is complex and highly variable. The light-curves of that object have been fitted using a model which includes the white-dwarf, a heated secondary and a point-like accretion region. The secondary emission contributes significantly even in optical wavelengths. This model also reproduces the main features of the optical polarization of 1RXS J231603.9–052713. We estimate the main parameters of the binary, of the accretion region and the distance to the system. An improved description of this system should include an extended and inhomogeneous accreting region as well as non-radial accretion.

**Key words:** novae, cataclysmic variables – polarization – stars: magnetic fields

## 1 INTRODUCTION

Cataclysmic variables (CVs) are short period binaries consisting of a white-dwarf (primary) and a late-type main-sequence star. The secondary star fills its Roche lobe, losing material to the primary by the inner Lagrangian point,  $L_1$ . Due to its angular momentum and viscous processes, this material forms an accretion disc around the white-dwarf. Polars, also called AM Her systems after their prototype, are CVs in which the primary has a magnetic field in the 10 to 200 MG range. In these systems the material from  $L_1$  follows a ballistic trajectory on the orbital plane (horizontal stream) up to the magnetic coupling region. From this region on the gas flow effectively traces the geometry of the magnetic field, forming an accretion stream. Unlike non-magnetic CVs, no disc is formed. Another consequence of the strong magnetic field is the synchronization of

the white-dwarf rotation with the orbital revolution. The variety of physical processes occurring and many open issues regarding the details of the emission components in these systems make them very interesting targets for astrophysical research. Reviews on polars can be found in Cropper (1990) and Warner (1995).

In the accretion region, near the white-dwarf surface, the material is fully ionized producing highly polarized cyclotron emission due to the presence of a strong magnetic field. As a large fraction of the optical flux in polars comes from this region, it shows large polarization, both linear and circular. Consequently, polarimetry is a fundamental tool to classify an object as an AM Her system.

Stokes parameters are also powerful to diagnose the state of the accreting region because they depend strongly on the angle by which that region is observed as well as on its physical properties. If the accretion region is small, the orbital behavior of the linear polarization position angle can be described by a simple equation that depends on the inclination of the system,  $i$ , and the colatitude of the axis of the magnetic field,  $\beta$ . Besides the quantities mentioned above, the phase interval during which no cyclotron emission is ob-

<sup>\*</sup> Based on observations made at the Observatório do Pico dos Dias, Brazil, operated by the Laboratório Nacional de Astrofísica.

<sup>†</sup> E-mail: claudiavr@das.inpe.br

served also constrains  $i$  and  $\beta$ . Estimates of the value of the magnetic field as well as of some other plasma properties can also be obtained through the modelling of flux and polarization variations with orbital phase (see Wickramasinghe & Meggitt 1985 and references therein on accreting column cyclotron models).

The fall of the column material onto the white-dwarf surface produces hard X-ray emission mainly through bremsstrahlung which is reprocessed as thermal soft X-ray emission. Consequently, *ROSAT* satellite has discovered many polars, contributing significantly to the number of known systems (see Schwope et al. 2000a, for instance).

In this work, we present new data for *ROSAT* polar candidates:  $R_C$  band polarimetry of 1RXS J161008.0+035222 and  $R_C$  and  $I_C$  band polarimetry and  $H$  band photometry of 1RXS J231603.9–052713. Some modelling of the objects is also presented. Preliminary results of these observations were presented in Rodrigues et al. (2005).

## 2 OBSERVATIONS AND DATA REDUCTION

In the following sections, we describe the acquisition and reduction of the polarimetric and infrared data. A summary of all observations is presented in Table 1.

### 2.1 Optical polarimetry

The observations have been performed with the 1.6-m Perkin-Elmer telescope at the *Observatório do Pico dos Dias* (OPD), Brazil, operated by the *Laboratório Nacional de Astrofísica* (LNA), Brazil. We have used a CCD camera modified to contain a polarimetric module described in Magalhães et al. (1996). The instrument consists of a fixed analyzer (calcite prism), a  $\lambda/4$  retarder waveplate and a filter wheel. The retarder plate is rotated in  $22^\circ.5$  steps. A complete measurement consists of eight images in consecutive retarder orientations. The calcite block separates the extraordinary and ordinary beams by  $12''$ . This technique eliminates any sky polarization (Piirola 1973; Magalhães et al. 1996). The  $\lambda/4$  retarder allows us to measure circular and linear polarization simultaneously. The CCD arrays were SITe back-illuminated devices, with  $1024 \times 1024$  pixels.

The images have been reduced following standard procedures using IRAF<sup>1</sup>. The extracted counts for the individual beams were used to calculate the polarization using the method described in Magalhães, Benedetti & Roland (1984) and Rodrigues, Cieslinski & Steiner (1998). The polarimetric reduction was greatly facilitated by the use of the package PCCDPACK (Pereyra 2000). Photometry can be done combining the counts in the two beams. We performed differential photometry of our target using brighter and fainter comparison stars in the field.

Our main goal was to measure the circular polarization with an error of the order of 1% and a time resolution enough to appropriately sample the orbital variability. Therefore, we chose exposure times,  $t_{int}$ , in the 60–90 s range. In this way, a polarization measurement spans  $8 \times t_{int}$  plus the dead time. We would usually group the images in sequences of 8 images with no overlap (images 1 through 8, images 9 through 16 and so on). However, in order to

improve the temporal resolution, we have grouped the images with overlap (images 1 through 8, images 2 through 9 and so on). In this way, we have a time interval between two points of typically 130 s. However, it should be noted that the actual time resolution is worse than that, by a factor of  $\approx 6$ , since the points are not independent.

Each night we observed polarimetric standard stars (Serkowski, Mathewson & Ford 1975; Bastien et al. 1988; Turnshek et al. 1990) in order to calibrate the system and estimate the instrumental polarization. The measured values of the unpolarized standard stars were consistent with zero within the errors: consequently no instrumental correction was applied. Linear polarized and unpolarized standard stars also show insignificant values of circular polarization. Our measurements are available at <http://www.das.inpe.br/~claudia>. Data using a Glan filter were also collected to estimate the polarization measurement efficiency of the instrument. They indicate that no instrumental correction is needed. Unfortunately, we could not calibrate our measurements in order to know the correct sign of the circular polarization. However, we can distinguish polarization of different signs. The signs in the figures are the instrumental ones.

### 2.2 Infrared photometry

The data were obtained with the 0.6-m Boller & Chivens and 1.6-m Perkin-Elmer telescopes at OPD (see Table 1 for details). The instrument used to collect the data is the CamIV imager, based on a Hawaii 1k  $\times$  1k Rockwell Int. array. The image scale is 0.48 arcsec/pix in the 0.6-m telescope, with a field-of-view (FOV) of  $8' \times 8'$ , and 0.24 arcsec/pix in the 1.6-m telescope, with a FOV of  $4' \times 4'$ . All observations were done in the  $H$  band. Our Hawaii detector is operated with a gain of  $4.5 \text{ e}^-/\text{ADU}$  and has a rms read-out noise of  $14.5 \text{ e}^-$ .

The telescope was offset between exposures by 10–20 arcsec to provide estimates of the sky background level by taking the median values of the images at each point. The resulting time series is not equally spaced in time, but has a time resolution that is quite sufficient for exploring the presence of the orbital modulation expected either from ellipsoidal variations or aspect variations from an asymmetrically heated secondary star.

The data reduction was carried out under IRAF and consists of the following steps:

**LINEARIZATION OF THE IMAGES.** A simple quadratic model with non-linear coefficient of  $3.6 \times 10^{-6}$  was applied to the raw counts in all pixels in all images. This value has been monitored since the beginning of the use of the detector on 2000 July, and has not changed;

**MASTER FLAT-FIELD IMAGE CONSTRUCTION (FOR EACH NIGHT).** For this, we obtained two sequences of 100 exposures of 2 s integration time; one with the dome flat-field lamp on and the other with the lamp off. The difference between the median-combined images (on-off) was normalized to unity and is the master flat-field image. Its rms measured in a  $[100:200, 100:200]$  section is  $\sim 5\%$  in all nights. The quality of the dome on-off flat-field image is comparable to what is obtained from taking the median values of all program images but it has the advantage of having been obtained from exactly the same number of images each night;

**BAD PIXEL MAP (BPM) CONSTRUCTION.** This is done by examining the histogram of the normalized master flat-field image. Pixels with response  $\leq 0.8$  or  $\geq 1.2$  are flagged as bad. Also, column 513 of the array is flagged for later interpolation with the task FIXPIX.

<sup>1</sup> IRAF is distributed by National Optical Astronomy Observatories, which is operated by the Association of Universities for Research in Astronomy, Inc., under contract with the National Science Foundation.

**Table 1.** Log of observations

Object	Date	Telescope	Instrument	Filter	Retarder	Integration time [s]	Time span [h]
1RXS J161008.0+035222	2003 Apr 22	1.6-m	CCD camera	$R_C$	$\lambda/4$	90	2.4
	2003 Apr 23	1.6-m	CCD camera	$R_C$	$\lambda/4$	80	3.6
	2003 Apr 26	1.6-m	CCD camera	$R_C$	$\lambda/2$	60	4.2
1RXS J231603.9–052713	2003 Jul 04	0.6-m	CamIV	$H$	-	60	2.8
	2003 Jul 05	0.6-m	CamIV	$H$	-	60	2.1
	2003 Jul 06	0.6-m	CamIV	$H$	-	60	2.5
	2003 Sept 24	1.6-m	CCD camera	$R_C$	$\lambda/4$	80	3.3
	2003 Sept 28	1.6-m	CCD camera	$I_C$	$\lambda/4$	90	1.3
	2004 Jun 22	1.6-m	CamIV	$H$	-	30	1.6
	2004 Jun 23	1.6-m	CamIV	$H$	-	30	1.7
	2004 Jul 28	1.6-m	CamIV	$H$	-	30	2.1
	2004 Oct 06	1.6-m	CCD camera	$R_C$	$\lambda/4$	90	2.1
	2004 Oct 07	1.6-m	CCD camera	$R_C$	$\lambda/4$	90	5.2
	2004 Oct 08	1.6-m	CCD camera	$R_C$	$\lambda/4$	90	6.0
	2004 Oct 09	1.6-m	CCD camera	$I_C$	$\lambda/4$	90	4.3

The extraction of the differential light-curves is as follows. Take for example the  $j^{th}$  image in the sequence of images obtained in one night. A “local” sky is built from the median of  $N_{sky}$  images around the  $j^{th}$  image in the series. The  $j^{th}$  image itself is included in this sky estimate. We verified that  $N_{sky} = 7$  gives good results. The sky image is subtracted from the  $N_{sky}$  images centred in image  $j$  and each one is divided by the master flat-field image and masked with the BPM. With the aid of the position of the reference star in each image, all  $N_{sky}$  images are registered to the position of the  $j^{th}$  image, combined, and the photometry of the resulting combined image is performed with `PHOT/IRAF`. The Heliocentric Julian day, reference star raw magnitude and magnitude differences of the target and comparison stars are output to a file. The image index is incremented to  $j + 1$  and the procedure is repeated. The processing of a whole night of data does not need the user’s intervention. Both the beginning and the end of the sequence of the images fail to have the  $j^{th}$  image centred on the sky estimate. We simply use the first (or last)  $N_{sky}$  images until (after) image  $N_{sky}/2 + 1$  (or  $j_{last} - N_{sky}/2$ ) is reached.

The combination of images improves the quality of the extraction at the expense of a poorer time-resolution in the light-curve. In our case, the time resolution is about 8 minutes in 2003 and 5 minutes in 2004. Both are good enough to sample phenomena that are expected to have typically  $\gtrsim 100$  minutes of time-scale.

### 3 1RXS J161008.0+035222

1RXS J161008.0+035222 is a *ROSAT* source presented in Schwöpe et al. (2000a), who have already quoted it as a possible AM Her system. Its optical identification and spectral classification as a potential magnetic CV were made by Jiang et al. (2000) and Schwöpe et al. (2002). These spectra show evidence of a M5 V secondary star. In spite of having an estimate for its orbital period of 0.13034 d (Schwöpe et al. 2002), no light-curve has been published.

#### 3.1 Results from optical photometry and polarimetry

Figure 1.a shows the calibrated light-curve obtained from the differential photometry of 1RXS J161008.0+035222 with respect to the star USNO B1.0 0938–0260775 ( $R_C = 17.1$  mag).<sup>2</sup> The typical uncertainty of the points is 0.03 mag. There are three estimates to the  $R_C$  magnitude of 1RXS J161008.0+035222 in the USNO catalogues:  $R_C = 15.8$  mag (USNO A2.0 0900–8458221), and  $R1 = 16.3$  mag and  $R2 = 18.99$  mag (USNO B1.0 0938–0260772). The comparison of our measurements with the USNO magnitudes suggests that the object was in the high-state during our measurements. This is consistent with the finding of Schwöpe et al. (2002) that the light-curve shows a quasi-sinusoidal shape associated to the object’s high mass-transfer state.

Our data can be used to constrain the ephemeris of 1RXS J161008.0+035222. The published period of 0.13034 d (Schwöpe et al. 2002) is inconsistent with our data: using this value the minima are out-of-phase. Therefore we have performed a period analysis that provides the following ephemeris for the time of minimum flux in the  $R_C$  band:

$$T_{min}(HJD) = 2\,452\,752.756\,7\,(70) + 0.132\,32\,(4)\,E. \quad (1)$$

This was calculated using a DFT algorithm as in Deeming (1975). The errors were estimated by a chi-square fitting of a sinusoidal curve to the observational data. Other methods, CLEAN (Roberts, Lehar & Dreher 1987) and the PDM in IRAF, give periods of 0.13229 d and 0.13241 d, respectively.

Figure 1 also shows the circular (panel b) and linear polarization (panel c) as well as its position angle (panel d). This object shows high values of circular polarization clearly modulated with the orbital period. This indicates that a cyclotron component is a significant part of the total flux of the system in the  $R_C$  band. Therefore, 1RXS J161008.0+035222 is definitely a polar.

The photometry and circular polarimetry are consistent with a

<sup>2</sup> The USNO accuracy is approximately 0.3 mag (Monet et al. 2003).

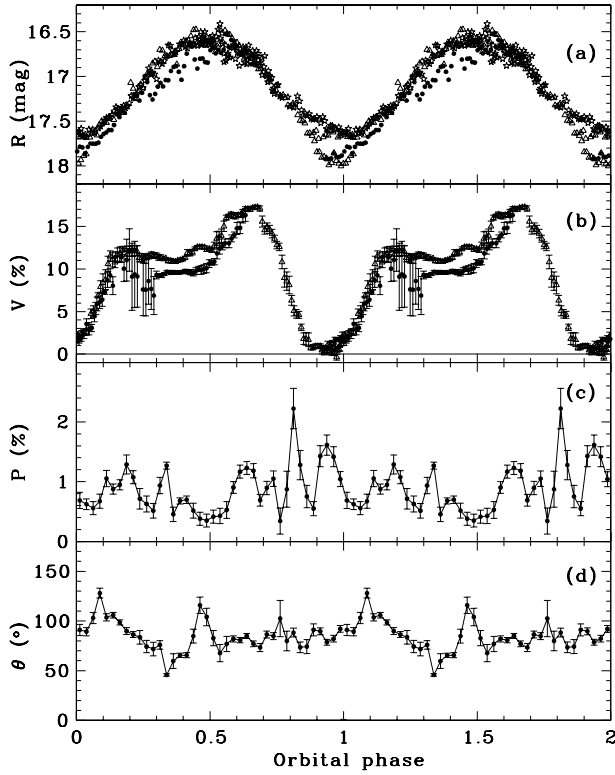


**Figure 1.** Observations of 1RXS J161008.0+035222 in the  $R_C$  band done in 2003 April. (a) Photometry, (b) circular and (c) linear polarization, and (d) polarization position angle. The different symbols in panels (a) and (b) represent distinct days of observations: full dots stand for April 22, open triangles stand for April 23 and open stars stand for April 26. In panels (c) and (d) the data from all days were binned in 40 phase intervals. These data were plotted assuming the ephemeris of Eq. 1. The circular polarization sign is the instrumental one.

one-pole accretion geometry in which the accretion region is never out of sight, so no occultation by the white-dwarf occurs.

The linear polarization is small along all orbital phases and shows no conspicuous peak - the point in the binned curve at  $\sim \Phi_{orb} = 0.8$  is not significantly above the statistical fluctuations. We expect peaks in the linear polarization when the column is seen edge-on as it rotates in or out of view over the limb of the white dwarf primary. Hence the absence of linear polarization peaks is also consistent with an one-pole geometry.

The foreground polarization produced by the interstellar dust in the line of sight to 1RXS J161008.0+035222 was estimated using the data of 2003 Apr 26 collected with a  $\lambda/2$  retarder. The weighted average of the linear polarization of 52 stars in the field is  $0.442 \pm 0.065\%$  at  $82.0 \pm 4.2^\circ$ : the quoted errors are the standard deviation of one measurement. The observed position angle of 1RXS J161008.0+035222 is approximately constant. This indicates that the measured linear polarization is small but not exactly equal to zero - in which case the position angle should have been randomly distributed between 0 and  $180^\circ$ . If we average all the phases of 1RXS J161008.0+035222, we obtain  $0.667 \pm 0.017\%$  at  $78.7 \pm 0.7^\circ$ . The similarity between the position angles indicates that the observed linear polarization of 1RXS J161008.0+035222

could have an interstellar origin. We will return to this discussion in the next section.

### 3.2 Modelling the flux and polarization

We can go a step further trying to fit a very simple model to 1RXS J161008.0+035222. We consider two components to the system emission: one has a constant and unpolarized flux; the second is cyclotron plus free-free in origin, and represents a point-like accretion region in the white-dwarf surface. The fluxes and polarizations (linear and circular) of the latter component are those from Wickramasinghe & Meggitt (1985, hereafter WM85). Recently, improved calculations of cyclotron emission in the accretion columns of polars have been presented (Potter et al. 2002; Potter et al. 2004). However, they are not available in tabular format, so we could not use them in our calculations. To compare the model with the observations, the maximum observed flux was normalized to unity. No normalization is needed to compare the polarimetric data with the model. A multiplicative factor for each component (WM85 and unpolarized) is calculated forcing the total model flux at the time of maximum light to be 1. The models have been calculated for a wavelength of  $6400 \text{ \AA}$ .

We produced a grid of models varying the magnetic field, the inclination of the system,  $i$ , and the colatitude of the magnetic field axis,  $\beta$ , for the eleven WM85 tables. We then fitted the models to the data. Each fit produces three  $\chi^2$  values. Each of them compares theoretical predictions with the observed intensity, linear and circular polarization data. The models which presented small values of the three  $\chi^2$  were inspected visually. Two regions in the parameters space produce models able to fit the observed flux and circular polarization. Two illustrative models of each region are shown superimposed on the data in Fig. 2 (panels a, b and c): model i is represented by a full line; and model ii, by a dot-dashed line. Sample model parameters are:

- (i)  $i = 2^\circ$ ;  $\beta = 1^\circ$ ;  $|B| = 10 \text{ MG}$ ;  $T = 40 \text{ keV}$ ; and  $\Lambda = 10^5$ ;
- (ii)  $i = 58^\circ$ ;  $\beta = 22^\circ$ ;  $|B| = 8.5 \text{ MG}$ ;  $T = 10 \text{ keV}$ ; and  $\Lambda = 10^7$ .

The parameter,  $\Lambda$ , is the optical depth parameter and depends on the path length, electron number density and magnetic field (WM85). We added the foreground polarization obtained in section 3.1 to the linear polarization of the models. The proportion of unpolarized to WM85 components in models i and ii are 0.26/0.74 and 0.22/0.78, respectively. Using the same geometry of model i, reasonable fits are also obtained with  $|B| = 16 \text{ MG}$ ,  $T = 40 \text{ keV}$  and  $\Lambda = 10^3$  or  $|B| = 20 \text{ MG}$  and the 20 keV shock front model of WM85. The main difference between the two models is the presence of a linear polarization peak around phase 0.5, which seems not to be present in the data. If the above solutions are valid, we can say that the magnetic field in 1RXS J161008.0+035222 is in the range 10–20 MG. The lack of a proper treatment of absorption/scattering in the accretion flow by WM85 can modify substantially the results in the phase interval 0.7 – 1.3.

In a radial and point-like model for the polarized component, the position angle of the linear polarization is a function of two geometric parameters,  $i$  and  $\beta$  (Stockman 1977; Brainerd & Lamb 1985). This happens because the polarization position angle is parallel or perpendicular to the projected angle of the magnetic field, which is parallel to the accretion column. Fig. 2 (panels c and d) shows the results for the linear polarization which was considered as the sum of the model and a foreground component represented

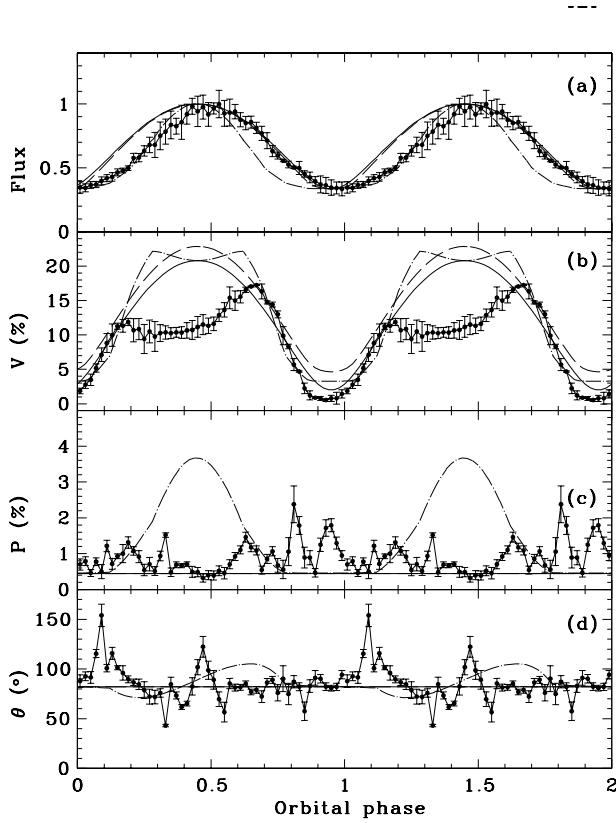


**Figure 2.** Simple models fit to 1RXS J161008.0+035222. The continuous and dot-dashed lines represent the point-like cyclotron emission region models i and ii, respectively (see text). A model with an extended region of  $1^\circ \times 10^\circ$  is shown by the dashed line (see text). The points represent all the available data binned in 50 phase intervals.

by the field stars average. As the linear polarization of model i is approximately zero, the resultant polarization is that of the field stars (a constant module and angle with phase). For model ii, a peak reaching more than 3% is produced. As this peak is not observed in the data, we favour the interpretation that the accretion region is seen approximately from top in any orbital phase. However, due to the simple assumptions of our models, the exact values of the inclination,  $i$ , and the magnetic colatitude,  $\beta$ , of model i should be interpreted with care. A spectroscopy study of this object can be helpful in constraining the viewing angle to the column.

We forced the time of inferior conjunction of the accretion column to be at phase 0.95. This was done in order to better fit the circular polarization. A slightly different choice (values nearer 1.0) could improve the flux fit instead, shifting the models to later phases (see Fig. 2). This small disagreement in phasing between polarization and flux data could be due to the variation of the phase of photometric minimum from night to night which is illustrated in Fig. 1.

To examine the influence of an extended emission region, we have done some additional modelling. We have used a grid of 25 points ( $5 \times 5$ ) to represent a rectangular region of arbitrary sides. All the points have the same emission properties. Considering  $i = 2^\circ$  and  $\beta = 1^\circ$  (as in model i) and an emission region extending  $1^\circ$  in latitude and  $10^\circ$  in longitude, the model produces results very similar to what the point-like model does, but the minimum of the

circular polarization is shallower than the observed (Fig. 2, dashed line).

The harmonic number of the cyclotron emission can be calculated using the adopted geometric model and the observed polarizations. Specifically, it is proportional to the ratio between circular and linear polarizations. The harmonic number is also inversely proportional to the magnetic field strength, which can then be calculated from the polarization ratio (see Wickramasinghe & Meggitt 1982 for the theory and Cropper, Menzies & Tapia 1986 for an example of application). We obtained for 1RXS J161008.0+035222 data harmonic numbers around  $10^{-3}$ , which is obviously incorrect. A more consistent result would be obtained if the linear polarization (produced by the cyclotron emission) was smaller than the observed. This could be the case if the observed linear polarization was not produced in the accretion region but had a different origin, as in the interstellar medium, as previously discussed.

In the above discussion we considered that flux modulation is totally originated from the cyclotron emission. The results can be modified if there is another source of modulated emission in  $R$  band in the system.

It should be noted that a more realistic model for the accretion region must include an inhomogeneous and extended structure. Such refinements could produce irregular, asymmetric curves as observed in polars in general, and also in 1RXS J161008.0+035222.

#### 4 1RXS J231603.9–052713

1RXS J231603.9–052713 is also a polar candidate from *ROSAT* (Beuermann & Thomas 1993; Thomas et al. 1998; Schwöpe et al. 2000a). No optical study has been published on this object so far. The orbital period quoted in Downes et al. (2001) catalogue is 0.145 45 d (Thomas H.-C., 2004, private communication).

##### 4.1 Orbital period determination

The distribution of the observing runs in 2003 was such that one cannot unambiguously count the number of orbital cycles to the 2004 season. A provisional value for the period of the orbital modulation from the combined optical and infrared data in 2003 is  $0.146\,13 \pm 0.000\,14$  d. This is marginally consistent with the value in Downes et al. (2001) and a good starting point to analyze the 2004 data. As shown in Fig. 3, the shape of the orbital modulation does not vary dramatically with wavelength, allowing us to combine the optical and  $H$  band data in a single set for the period analysis. Starting from the 0.146 13 d period value for 2003, we find a minimum phase dispersion for both optical and infrared data for the ephemeris:

$$T_{min}(HJD) = 2\,452\,825.837\,6(30) + 0.145\,451\,6(10) E. \quad (2)$$

##### 4.2 Results from photometry and polarimetry

Figure 3 shows the photometric data folded using the ephemeris of Equation (2). The optical magnitudes of 1RXS J231603.9–052713 have been calculated using USNO B1.0 0845–0644672 as a calibrator ( $R_2 = 14.1$  mag,  $I_2 = 13.43$  mag). The  $H$  band magnitudes are relative to 2MASS 23161253–0529164 ( $H = 11.609 \pm 0.025$  mag) in 2003, and relative to 2MASS 23160010–0526237 ( $H = 12.498 \pm 0.025$  mag) in 2004.

In September, 2003, the  $R_C$  band flux of

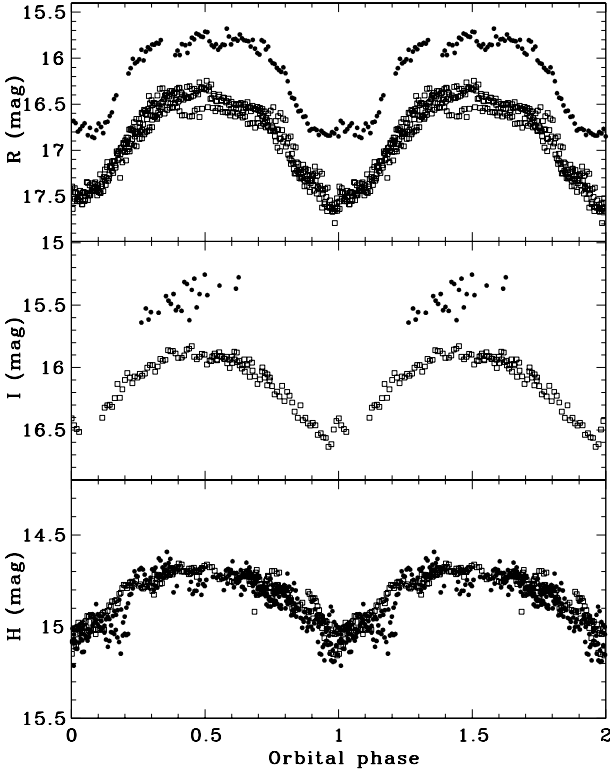


**Figure 3.** Optical and NIR photometry of 1RXS J231603.9–052713: the dots were used for 2003 data and open squares for 2004 data. The optical and IR data are not simultaneous.

1RXS J231603.9–052713 was twice its value in October, 2004, suggesting a higher accretion state in 2003. In spite of the poor quality of the  $I_C$  band data in 2003, they also indicate a higher luminosity in 2003. We discarded a flux variation in the main comparison star by verifying its flux relative to other field objects. The USNO B1.0 photometry of the 1RXS J231603.9–052713 (USNO B1.0 0845–0644683) is  $R1 = 18.550$  mag,  $R2 = 17.190$  mag and  $I2 = 17.070$  mag. The  $H$  band flux does not show year-to-year variation, and the 2MASS catalogue value ( $H = 14.798$  mag at  $\phi_{orb} = 0.33$ ) is consistent with our data: the long-term variable component is far less prominent at  $1.6\mu\text{m}$ . However, one should recall that the  $H$  band data are not simultaneous with the  $R_C$  and  $I_C$  data. The  $H$  band light curve is consistent with the heating of the secondary by the primary being important in this system, as seen in other CVs. It can also be seen that the amplitude of the orbital modulation decreases for longer wavelengths.

Figures 4 and 5 show the circular and linear polarimetry of 1RXS J231603.9–052713 in the  $R_C$  and  $I_C$  bands, respectively. In both filters, we measured large, strongly variable circular polarization, confirming this object as a polar. In Figure 4 all the data from a given year were binned in 50 orbital phase intervals to provide a better visualization. The variability of this object is illustrated in Figure 6 which shows daily circular polarimetry without any binning.

As for 1RXS J161008.0+035222 no change of sign in the circular polarization is observed. 1RXS J231603.9–052713 seems, however, to have a more complex accretion geometry. Therefore the

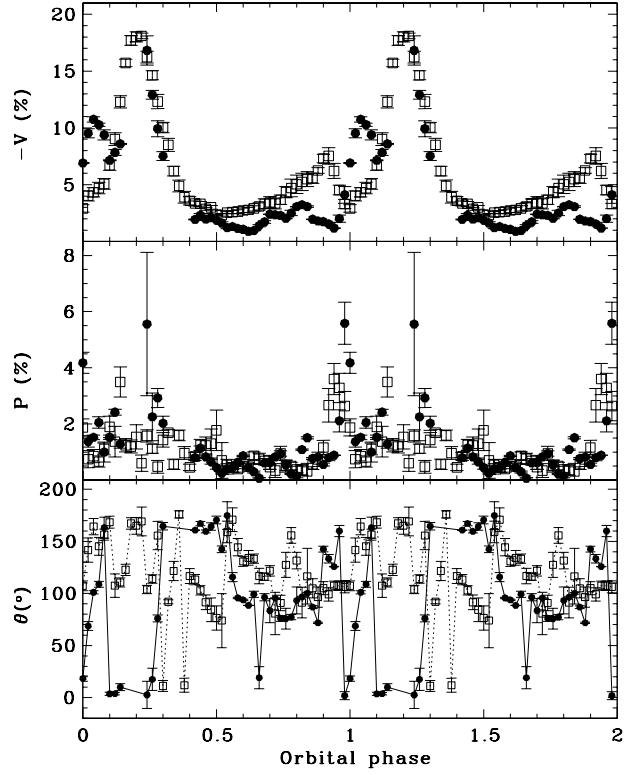


**Figure 4.** Circular and linear polarimetry of 1RXS J231603.9–052713 in the  $R_C$  band. The data were binned in 50 phase boxes. Dots stands for 2003 data and open squares, for 2004 data. The circular polarization sign is the instrumental one.

suggestion of a one-pole geometry could be incorrect. In a dipolar magnetic geometry, the possibilities are: (1) a single pole visible; (2) two poles with the same polarity; or (3) one pole observed from the top, with the other seen upside down.

The  $R_C$  band circular polarization presents a maximum of constant amplitude near phase 0.2. The interval  $0.4 < \phi_{orb} < 0.6$  shows small circular polarization. From phase 0.7 to 1.1 the polarization varies significantly, presenting variable peaks at different phases in different occasions.

The phasing of the flux and polarization curves, the asymmetric profile, and the highly changeable circular polarization makes 1RXS J231603.9–052713 a very interesting object. These properties resemble QQ Vul (Cropper 1998; Schwöpe et al. 2000b) and may be originated by a complex and variable accretion geometry.

#### 4.3 Modelling the optical flux and polarization: a cyclotron model

Following the same procedure described in the previous section for 1RXS J161008.0+035222, we tried to fit the  $R_C$  band data with a simple model of a non-polarized component plus a cyclotron and free-free emitting region represented by the WM85 models. Considering only the light-curve, we could identify two families of models: (1) the photometric minimum corresponds to the time when the accretion column has the smallest angle with the line of sight and is caused by intrinsic properties of the accreting region; or (2) the minimum occurs when the column points away from the

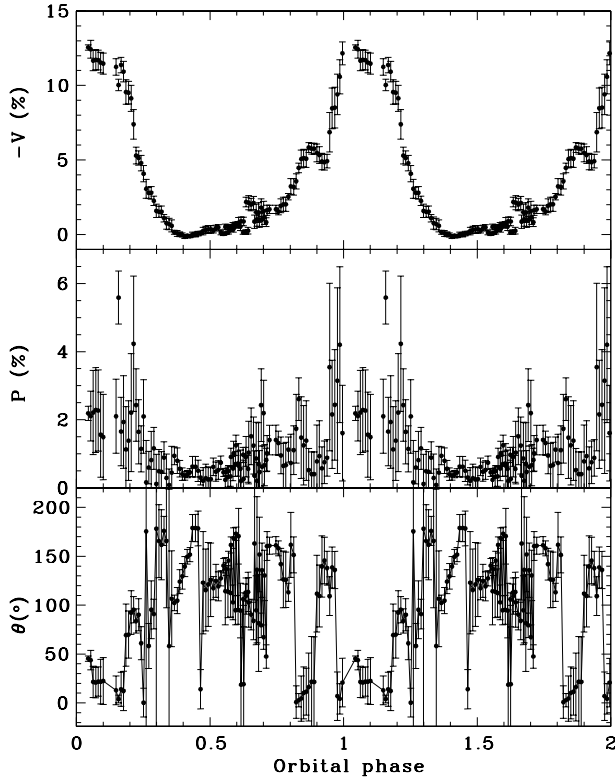


**Figure 5.** Circular and linear polarimetry of 1RXS J231603.9–052713 in the  $IC$  band for 2004 October. No binning was applied. The circular polarization sign is the instrumental one.

observer and is caused by occultation of the accreting region by the white-dwarf.

We discard the second family of models for many reasons. First, the model fluxes fit the light-curve poorly. In addition, the accretion column in polars tends to be located near the plane perpendicular to the orbit and connecting the two stars (Liebert & Stockman 1985). Also, if the  $H$  band light-curve is due to a heated secondary, the phasing would be wrong.

Hereafter, we consider only the first family of models. They provide inclinations of around  $30$ – $50^\circ$ , colatitudes of the magnetic axis ranging from  $20$  to  $30^\circ$  and a magnetic field strength of  $20$ – $30$  MG. These models reproduce very well the light-curve, but not the circular polarization curve. In Figure 7 (dashed line) we show one such a model. It is clear that the predicted polarization is larger than the observed: no alternative choice of parameters can improve the fit. A possible solution is to consider that part of the flux modulation comes from a non-cyclotron source. To test this hypothesis, we have constructed a model with a third component having the same modulation of the observed curve, but with a free scale factor. We could then reproduce well the light-curve and the circular polarization peak in phase  $0.2$ . (Figure 7, solid line). In Section 4.4, we return to this discussion using a plausible model for the modulated component.

The variation of position angle cannot be described using the standard radial accretion geometry of Stockman (1977). Cropper (1989) has calculated the behavior of the position angle with orbital phase for accretion along the lines of a dipolar magnetic field. The departure from the radial model tends to be larger for small values

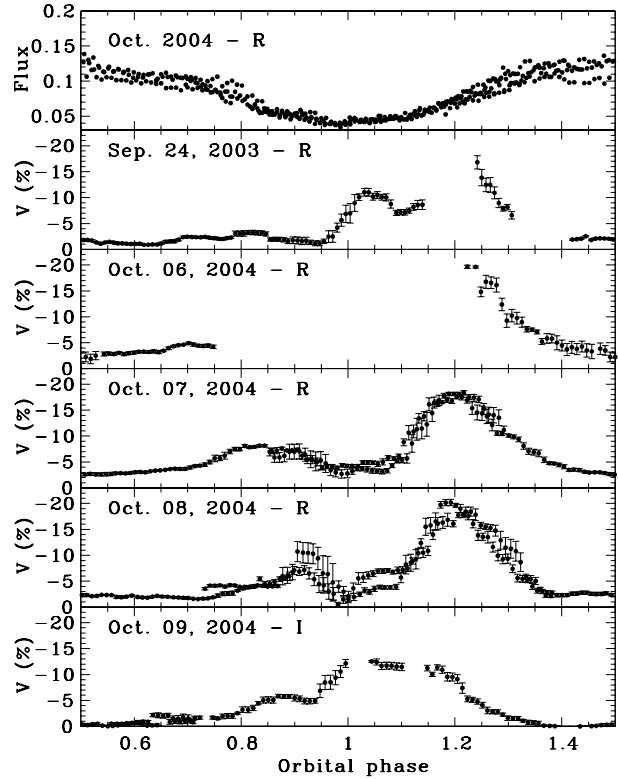


**Figure 6.** Circular polarimetry of 1RXS J231603.9–052713. Each panel represents the data for one day of observation. The first panel presents the  $R_C$  band flux (in arbitrary units) in 2004 October 06–09. No binning was applied. The circular polarization sign is the instrumental one.

of the threading radius - the radius where the magnetic field line crosses the orbital plane - (see his Figs. 3 and 4). Therefore, the monotonic increase in position angle near phase  $0.0$  and  $0.25$  in 2003 data could be interpreted as non-radial accretion with a small threading radius ( $\lesssim 50$  radius of the white-dwarf). Alternatively, the occurrence of two of these features may indicate the presence of two accreting regions.

#### 4.4 Modelling the optical and infrared flux: a cyclotron model plus a heated secondary

As shown in the previous section, there is a suggestion of a modulation in the  $R_C$  band originated by non-cyclotron emission. A potential source would be the contribution from the heated secondary star. This hypothesis is studied below using the code presented in Appendix A, which includes (1) the white-dwarf contribution, (2) a heated secondary star, and (3) an arbitrary component which we have selected from the grid of models from WM85.

A first attempt to fit the  $R_C$  and  $H$  band photometry with a simple model in which only the secondary star (including heating effect) and white-dwarf were present failed in the sense that too much  $R_C$  flux is predicted if we fit the  $H$  band data. It indicates that a third component exists even in the NIR. This is not surprising since we know that there is additional light in optical wavelengths from cyclotron emission in this binary. If this cyclotron emission is also present in the  $H$  band, we have one more constraint to the magnetic field ( $B$ ) value, since that emission occurs at wavelengths

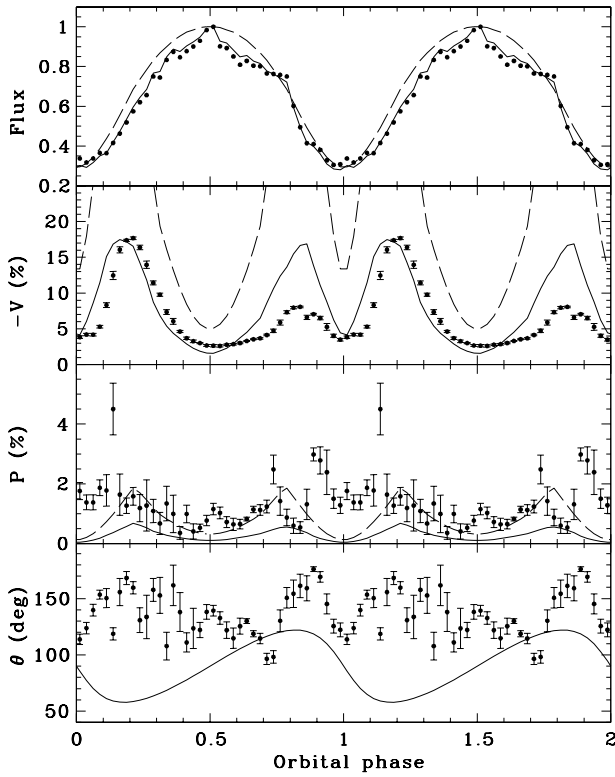


**Figure 7.** Sample fits for 1RXS J231603.9–052713  $R_C$  band data from Oct 07, 2004. The dashed line represents a two-component model: WM85 plus a constant and non-polarized emission, in which the WM85 responds for 73% of the maximum flux. The solid line is a three-component model: WM85 (24% at maximum light), a non-polarized constant flux (25%) and a non-polarized modulated emission (51%). In both models the parameters of the WM85 component are:  $i = 40^\circ$ ;  $\beta = 20^\circ$ ;  $|B| = 23$  MG;  $T = 10$  keV;  $\Lambda = 10^7$ .

larger than a given limit inversely proportional to  $B$ . This discards models with large values of  $B$ .

We chose two models (from the first family as defined in Sec. 4.3) from the grid of WM85 that describe the polarimetry reasonably well, but have distinct behavior in the near infrared: the first is constant in the  $H$  band. They have the following parameters:

- (i)  $i = 40^\circ$ ,  $\beta = 20^\circ$ ,  $|B| = 23$  MG,  $T = 10$  keV,  $\Lambda = 10^7$  (Figure 7);
- (ii)  $i = 40^\circ$ ,  $\beta = 30^\circ$ ,  $|B| = 27.1$  MG,  $T = 10$  keV,  $\Lambda = 10^6$ .

The analysis below takes into account the simultaneous fit of the light-curves in the  $R_C$ ,  $I_C$  and  $H$  bands. We incorporated the cyclotron contribution into our model, fixing its fraction relative to the total light at  $\phi_{orb} = 0.5$  to be 0.25 in the  $R_C$  band. In the other bands, we fix the cyclotron contribution in such a way that the proportion relative to the  $R_C$  band is that given by the WM85 models. The inclination of the system is fixed at 40 degrees, to be consistent with the polarimetric models chosen from the WM85 tables. The results depend very little on the inclination for the 30–50 degrees range. All modelling assumes the primary to follow the Hamada-Salpeter mass-radius relation. The allowed range of primary masses is  $0.4 - 1.1 M_\odot$ . The Roche-lobe filling star is forced to follow the mass-radius relation of Chabrier & Baraffe (1997).

**Table 2.** Parameters of the emission models for 1RXS J231603.9–052713 shown in Figures 8 and 9

Parameter	Model $i$	Model $ii$
$T_1$	55 575 K	54 626 K
$T_2$	3 280 K	3 320 K
$R_1/a$	0.0052	0.0053
$M_1$	$1.09 M_\odot$	$1.09 M_\odot$
$M_2$	$0.39 M_\odot$	$0.39 M_\odot$
Distance, $d$	416 pc	418 pc
$\chi$	15.57	15.45

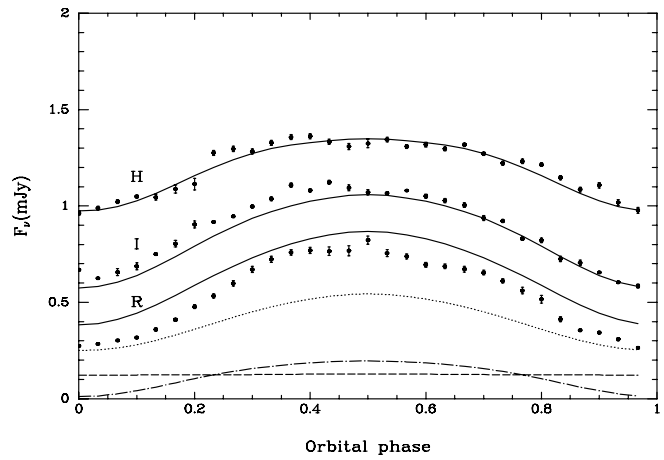


**Figure 8.** Heated secondary models of 1RXS J231603.9–052713 in the  $R_C$ ,  $I_C$ , and  $H$  bands for model  $i$ . The individual contributions are shown for the  $R_C$  band, with the ellipsoidal+heating component shown as a dotted line, the white-dwarf contribution shown as a dashed line and the cyclotron component as dot-dashed (model  $i$ ). The total flux is shown as a continuum line.

Reddening is assumed to be  $E(B - V) = 0.037$  estimated using the procedure from Schlegel, Finkbeiner & Davis (1998). Unless otherwise stated, the following discussion is valid for both polarimetric models.

We would like to note that our photometry is calibrated against the USNO B1.0 magnitudes of USNO B1.0 0845-0644672 ( $R_2 = 14.1$ ,  $I_2 = 13.43$ ). The conversion between  $R_2$  and Landolt's  $R_C$  for this object indicates a difference of only 0.02 mag (Kidger 2003). We assume the  $I_2$  magnitude also to be the same as Landolt's.

Table 2 shows the parameters obtained for the best fits for each WM85 model which are shown in Figures 8 and 9 superimposed in the  $H$ ,  $I_C$  and  $R_C$  band light-curves. The  $H$  and  $I_C$  fluxes are well fitted by the models, but the amplitude of the modulation in the  $R_C$  band model is smaller than the observed.

A word about the figure of merit used in the optimization of our models. We adopted  $\chi = \sqrt{\chi_R^2 + \chi_I^2 + \chi_H^2}$  where  $\chi_X^2 = \sum_{i=1}^N \frac{(O_i - C_i)^2}{\sigma_i^2}$  stands for  $\chi^2$  in the  $X$  band. The high values of  $\chi$  shown in Table 2 are due to the fact that the errors  $\sigma_i$  in the 30 phase bins take into account only the statistical uncertainties in the bins themselves. Flickering, for example, adds additional uncertainties that are not considered and could only be estimated with longer sets of data.



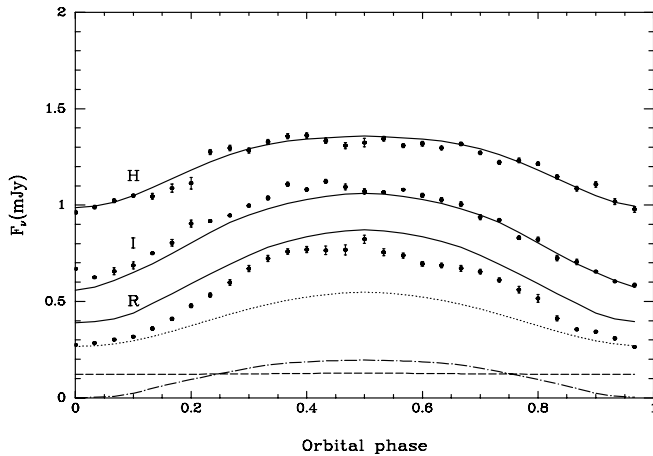


Figure 9. Same as in Figure 8, for model ii.

The temperature of the primary is large when compared with that observed in cataclysmic variables in general,  $\sim 16\,000$  K (Sion 1999) and its presence could in principle be detected photometrically, specially at  $\phi_{orb} = 0.0$  where it contributes with a fraction of about 50% in the  $R_C$  band. However, that high temperature source may be better associated with a small region in the white-dwarf photosphere reprocessing the emission produced in the accretion/shock region. Such a component is very important in polars and contributes in soft X-rays and ultraviolet wavelengths.

The temperature of the secondary star is 3 280 K for model i. For  $d = 416$  pc this corresponds to  $M_H = +7.5$  and spectral type in the range M3-M4 V. The contribution of the secondary star alone at  $\phi_{orb} = 0.0$  would be 0.871 mJy corresponding to  $H \sim 15.19$ . This is in good agreement with the observed minimum value of  $H = 15.07$  in the binned light-curve.

For model ii, with  $T_2 = 3\,320$  K we have an object slightly cooler than M3V and for  $d = 418$  pc, we have  $M_H = +7.14$  at  $\phi_{orb} = 0.0$ . Our model predicts a contribution of 0.903 mJy from the secondary star at  $\phi_{orb} = 0.0$ . This is equivalent to apparent  $H = 15.13$  and agrees well with the observed value.

Figure 10 shows a comparison of the results of model i with the observed spectral energy distribution (SED) at  $\phi_{orb} = 0.0$ . The comparison for model ii is not shown since it is visually identical to Figure 10. One can see that the  $H$  band measurement has the smallest uncertainty since our photometry was calibrated against 2MASS objects. The  $J$  and  $K_s$  band points are inferred from the 2MASS data. They were obtained from an interpolation of the amplitude of the photometric modulation (for the  $J$  band) and an extrapolation for the  $K$  band. The model amplitudes are 0.47 mag and 0.20 mag, for the  $J$  and  $K$  bands, respectively. The  $R$  and  $I$  measurements are from the USNO catalog, therefore, non-simultaneous with our  $H$  band measurement. The uncertainty in the  $R_C$  and  $I_C$  measurements comes from the USNO calibration and from the fact that these measurements are not simultaneous with the NIR data. The crosses and pluses in Figure 10 show the SEDs from measurements in 1991 and 1995 (Thomas et al. 1998 and Thomas, H.-C. private communication). The solid straight-line segments correspond to the output of our model (at  $\phi_{orb} = 0.0$ ) considering the sum of all components. Notice that at this phase we expect the smallest contamination from the heating of the secondary star. The

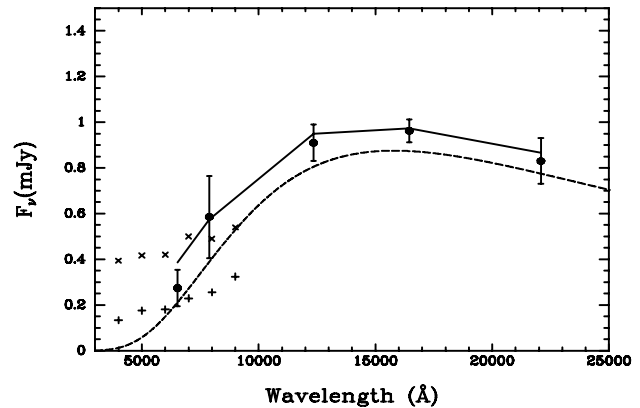


Figure 10. The spectral energy distribution for 1RXS J231603.9–052713 at minimum light (see text). Model i has been superimposed on the data. The dashed line represents a 3 280 K blackbody curve.

dashed curve shows the contribution of the secondary star if there was no heating from the white-dwarf.

Figure 11 shows the results for the  $I_C$  band applying the two best fits for flux and the WM85 models to calculate the polarization. As for the  $R_C$  band, the overall observed level and shape are reproduced, but the details of the curve needs a more refined modelling.

## 5 CONCLUSIONS

We present polarimetric data for two *ROSAT* candidates to AM Her systems: 1RXS J161008.0+035222 and 1RXS J231603.9–052713. Optical photometry of 1RXS J161008.0+035222 and optical/NIR photometry of 1RXS J231603.9–052713 were obtained. Both systems show high values of circular polarization confirming them as polars. We also presented new ephemerides for the two systems.

A simple model of a point-like accretion region in the white-dwarf plus a constant component is able to reproduce the gross features of 1RXS J161008.0+035222. It corresponds to a system seen approximately face-on, with a (dipolar) magnetic field aligned with the rotation axis of the white-dwarf. The magnetic field strength was estimated to be in the 10–20 MG range. Our model predicts small values for the linear polarization which are consistent with the data. Another possible model assumes an inclination around  $60^\circ$  and  $\beta \approx 20^\circ$ . The flux and circular polarization are well fitted, but the model linear polarization peak is not present in the data. The averaged linear polarization of 1RXS J161008.0+035222 is consistent with an interstellar origin, according to the polarimetry of field stars.

Our  $R_C$  band observations of 1RXS J231603.9–052713 have been taken in two different brightness states which show, however, similar light-curve shapes. The dependence of the  $R_C$  band polarization with the orbital phase shows considerable variation in time-scales of days or years, but its maximum is apparently constant around 20%. The secondary seems to be an important source of light even in the  $R_C$  band. We have presented a model that reproduces the main features of flux and polarization in all observed bands. It considers three components: a white-dwarf, a heated sec-

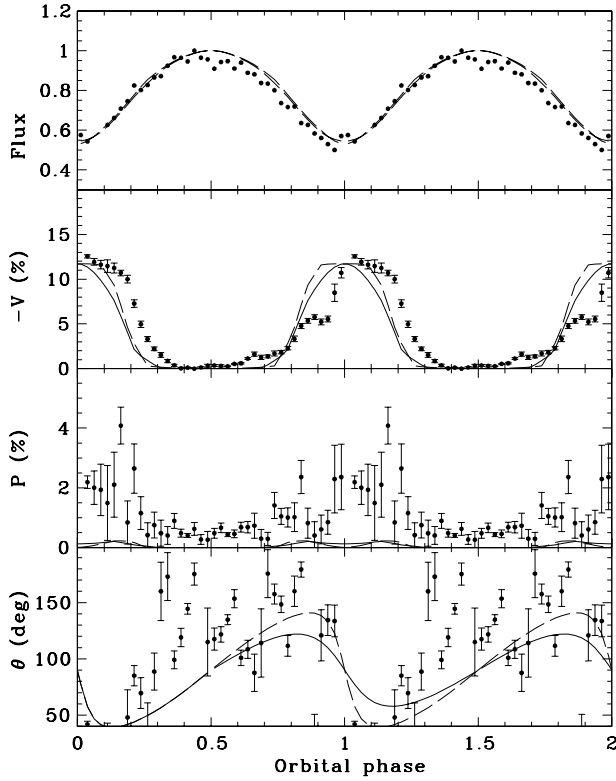


**Figure 11.** Resulting flux and polarization for 1RXS J231603.9–052713  $I_C$  band using the heated secondary model. The solid lines represents the model i results. The dashed line is used to shown the model ii.

ondary and an accretion column. The suggested parameters for the system are:  $T_1 \approx 54\,000\text{K}$  (probably associated with the accretion region);  $T_2 \approx 3\,250\text{K}$ ;  $R_1/a \approx 0.0052$ ;  $M_1 \approx 1.10M_\odot$ ;  $M_2 \approx 0.39M_\odot$ ; distance  $\approx 410\text{ pc}$ ;  $i \approx 40^\circ$ ;  $\beta = 20\text{--}30^\circ$ ;  $|B| = 20\text{--}30\text{ MG}$ . A point-like accretion region is clearly not enough to fit the asymmetry of the 1RXS J231603.9–052713 polarization. An extended and inhomogeneous accretion region may better reproduce the data. The position angle of the linear polarization suggests non-radial accretion in this system.

## ACKNOWLEDGEMENTS

We thank R. Downes for clarifying the catalogue entry information on the orbital period of 1RXS J231603.9–052713 and H.-C. Thomas for providing unpublished 1RXS J231603.9–052713 spectra. We also acknowledge an anonymous referee by his(her) suggestions. This work was partially supported by Fapesp (CVR: Proc. 2001/12589-1). This research has made use of: the USNOFS Image and Catalogue Archive operated by the United States Naval Observatory, Flagstaff Station (<http://www.nofs.navy.mil/data/fchpix/>); the SIMBAD database, operated at CDS, Strasbourg, France; and the NASA's Astrophysics Data System Service.

## REFERENCES

- Bastien P., Drissen L., Menard F., Moffat A. F. J., Robert C., St-Louis N., 1988, *AJ*, 95, 900
- Beuermann K., Thomas H.-C., 1993, *Adv. Space Res.*, 13(12), 115
- Brainerd J. J., Lamb D. Q., 1985, in Lamb D. Q., Patterson J., eds., *Cataclysmic Variables and Low-Mass X-Ray Binaries*. D. Reidel Publ. Company, p. 247
- Chabrier G., Baraffe I., 1997, 1997, *A&A*, 327, 1039
- Claret A., 1998, *A&A*, 335, 647
- Cropper M. S., 1989, *MNRAS*, 236, 935
- Cropper M. S., 1990, *Space Sci. Rev.*, 54, 195
- Cropper M. S., 1998, *MNRAS*, 295, 353
- Cropper M. S., Menzies, J. W., Tapia, S. 1986, *MNRAS*, 218, 201
- Deeming T. J., 1975, *Ap& SS*, 36, 137
- Downes R. A., Webbink R. F., Shara M. M., Ritter H., Kolb U., Duerbeck H. W., 2001, *PASP*, 113, 764
- Gilks W. R., Richardson S., Spiegelhalter D.J., 1996, *Markov Chain Monte Carlo in practice*, Chapman and Hall, Suffolk
- Jiang X. J., Engels D., Wei J. Y., Tesch F., Hu J. Y., 2000, *A&A*, 362, 263
- Kidger M. R., 2003, <http://www.iac.es/galeria/mrk/comets/USO.Landolt.htm>
- Liebert J., Stockman H. S., 1985, in Lamb D. Q., Patterson J., eds., *Cataclysmic Variables and Low-Mass X-Ray Binaries*. D. Reidel Publ., Dordrecht, p. 151
- Lucy L. B., 1967, *Zeitschrift fuer Astrophysik*, 65, 89
- Magalhães A. M., Benedetti E., Roland E., 1984, *PASP*, 96, 383
- Magalhães A. M., Rodrigues C. V., Margoniner V. E., Pereyra A., Heathcote S., 1996, in Roberge W. G., Whittet D. C. B., eds., *Polarimetry of the Interstellar Medium*. Astron. Soc. Pac., San Francisco, p. 118
- Monet D. G. et al., 2003, *AJ*, 125, 984
- Pereyra A., 2000. *Dust and Magnetic Fields in Dense Regions of the Interstellar Medium*, PhD Thesis, Univ. São Paulo
- Pirola V., 1973, *A&A*, 27, 383
- Potter S. B., Ramsay G., Wu K., Cropper M., 2002, in Gänsicke B. T., Beuermann K., Reinsch K., eds., *The Physics of Cataclysmic Variables and Related Objects*. Astron. Soc. Pac., San Francisco, p. 165
- Potter S. B., Romero-Colmenero E., Watson C. A., Buckley D. A. H., Phillips A., 2004, *MNRAS*, 348, 316
- Provencal J. L., Shipman H. L., Hog E., Thejll, P., 1998, *ApJ*, 494, 759
- Roberts D. H., Lehar J., Dreher J. W., 1987, *AJ*, 93, 968
- Rodrigues C. V., Cieslinski D., Steiner, J. E., 1998, *A&A*, 335, 979
- Rodrigues C. V., Cieslinski D., Jablonski F. J., D'Amico F., Steiner, J. E., Diaz, M. P., Hickel, G. R. 2005, in Adamson A., Aspin C., Davis C., Fujiyoshi T., eds., *ASP Conf. Ser. 343, Astronomical Polarimetry*. Astron. Soc. Pac., San Francisco, p. 401
- Rucinski S. M. 1969, *Acta Astron.*, 19, 245
- Schlegel D. J., Finkbeiner D. P., Davis M., 1998, *ApJ*, 500, 525
- Schwope A. D., Catalán M. S., Beuermann K., Metzner A., Smith R. C., Steeghs D., 2000b, *MNRAS*, 313, 533
- Schwope A. D., Hasinger G., Lehmann I., Schwarz R., Brunner H., Neizvestny S., Ugryumov A., Balega Yu., Trmper J., Voges W., 2000a, *Astronomische Nachrichten*, 321, 1
- Schwope A. D., Brunner H., Buckley D., Greiner J., Heyden K. v. d., Neizvestny S., Potter S., Schwarz R., 2002, *A&A*, 396, 895

Serkowski K., Mathewson D. L., Ford V. L., 1975, *ApJ*, 196, 261  
 Sion, E. M., 1999, *PASP*, 111, 532  
 Stockman H. S., 1977, *ApJ*, 218, L57  
 Thomas H.-C., Beuermann K., Reinsch K., Schwöpe A. D., Truemper J., Voges W., 1998, *A&A*, 335, 467  
 Thorstensen J. R., Armstrong E., 2005, *AJ*, 130, 759  
 Turnshek D. A., Bohlin R. C., Williamson R. L. II, Lupie O. L., Koornneef J., Morgan D. H., 1990, *AJ*, 99, 1243  
 Warner B., 1995, *Cataclysmic Variable Stars*. Cambridge Univ. Press, Cambridge  
 Wickramasinghe D. T., Meggitt M.A., 1982, *MNRAS*, 198, 975  
 Wickramasinghe D. T., Meggitt M.A., 1985, *MNRAS*, 214, 605  
 Zhang E.-H., Robinson E. L., Nather R. E., 1986, *ApJ*, 305, 740

## APPENDIX A: A MODEL FOR OPTICAL AND INFRARED FLUX IN CVS: WHITE-DWARF PLUS A HEATED SECONDARY

### A1 Light-curve modelling

Our code is similar to the one described in Zhang, Robinson & Nather (1986). The secondary star always fills its Roche lobe and the primary star is spherical. Both are treated as blackbodies.

The stars' surface are represented by a mesh of  $100 \times 100$  elements of area. Given a mass ratio, for each point of the grid corresponding to the secondary star, we calculate the parameters of the Roche equipotential surface. This allows us to compute the local gravity and the gravity darkening via  $T = T_{pole}(g/g_{pole})^\beta$ . Here  $T_{pole}$  is the temperature of the far pole of the secondary star. We follow Lucy (1967) and use  $\beta = 0.08$  for a typical secondary in a CV.

The effect of the irradiation of the primary star on the secondary is calculated with a simple approximation:  $T^4 = T_0^4 + (1 - a)F_{irr}/\sigma$ . Here  $T_0$  is the grid-point temperature without irradiation,  $a$  is the albedo of the secondary star,  $F_{irr}$  is the irradiation flux on the secondary and  $\sigma$  is the Stefan-Boltzmann constant. All points on the secondary visible from the spherical primary are affected by irradiation. Both the distance and projected areas of the respective surface grid elements are taken into account in the calculations. We use  $a = 0.5$  in our simulations, according to what is expected for convective stars (Rucinski 1969).

The limb-darkening is assumed to be linear, that is,  $I(\mu)/I_0 = 1 - u(1 - \mu)$ , where  $\mu$  is the cosine of the angle from the center to the border of the star, and  $u$  is the limb-darkening coefficient. Considering the range of wavelengths examined in our modelling we adopted  $u = 0.6$  for the secondary (Claret 1998). We followed Thorstensen & Armstrong (2005) and explored a range of values for the limb-darkening of the white dwarf. The results depend very little on the particular value and we chose  $u = 0.7$  for the primary.

Since the orbital period and masses of the components define the size of the binary, absolute dimensions of the grid elements can be used in the calculation of the flux in the direction of the observer. This means that the distance can be used as a parameter to be determined from the data. For a low-inclination system for which the secondary temperature is zero and a non limb-darkened spherical primary of  $1R_\odot$  with a temperature of 5000 K at a distance of 1 kpc, the model correctly predicts a flux of 2.05 mJy in the *V* band.

The output of the light-curve synthesis program is the sum of the flux components due to the secondary star (ellipsoidal variation plus heating of the secondary), the contribution of the white-dwarf and an optional third component (e.g., due to cyclotron emission)

whose fraction is a parameter that can be fixed or determined from the fit to the data, according to the information available.

The main advantage of a simplified light-curve synthesis code like ours is speed of execution. The fitted parameters are:

- (i) orbital inclination;
- (ii) temperature of the primary;
- (iii) pole temperature of the secondary;
- (iv) masses of the components;
- (v) distance;
- (vi) fraction of total light at  $\phi_{orb} = 0.5$  due to cyclotron emission.

The radius of the primary is forced to follow the Hamada-Salpeter relation for Helium white-dwarfs. The range of masses was limited to  $0.4 M_\odot < M_1 < 1.1 M_\odot$  according to the observed distribution of field white-dwarfs (Provencal et al. 1998)

The mass of the secondary was allowed to be in the range  $0.08 M_\odot < M_2 < 1.0 M_\odot$ . We forced the secondary star to follow the mass-radius relation of Chabrier & Baraffe (1997).

### A2 Monte Carlo Markov Chain

The approach of using Monte Carlo Markov Chains (MCMC) for the estimation of parameters has the advantage of a good flexibility on deciding which parameters are to be estimated or kept fixed and gives very robust intervals of confidence for the parameters. A review on MCMC can be found in Gilks, Richardson & Spiegelhalter (1996).

We used the MCMC to sample the *a posteriori* distribution of the parameters  $\Theta$  of our model as given by the Bayes theorem:

$$p(\Theta|D) \propto p(D|\Theta)p(\Theta),$$

where  $p(D|\Theta)$  is the usual likelihood of the data given the parameters  $\Theta$  and  $p(\Theta)$  is any prior information on the parameters. For example, if a system does not show eclipses,  $p(\Theta)$  may be considered null for inclination angles larger than  $\approx 70$  deg.

The marginalized distributions of the parameters of long Markov Chain allow us to derive their localization (e.g., via the mode of the distribution) and confidence intervals by simple integration along the distribution.